Interference and the art of static correction: raypath interferometry at Hussar

David C. Henley

ABSTRACT

The technique known as raypath interferometry has been developed specifically to provide static corrections for seismic data from areas where surface-consistency is not valid, and where near-surface conditions complicate reflection event arrivals. The new technique is also compatible with surface-consistent data, however, and can increase effective redundancy for static corrections in general. Furthermore, the interferometry process itself, which involves inverse filtering, can apparently broaden the band of the resulting stack image. We demonstrate raypath interferometry on a subset of data from the 2011 Hussar Low-frequency experiment, providing static corrections for both PP and PS data. The result for PP data appears to be at least as good as conventional statics, while that for PS data is at least comparable to the conventional results over key horizons.

INTRODUCTION

Static correction is a processing procedure used on most land seismic data to approximately remove the effects of variations in the thickness and velocity of the surface layer of the earth. These variations affect seismic reflections from deeper, more uniform layers in several ways, degrading the reflection event waveform through attenuation and scattering, and, most obviously, delaying reflection event arrivals at receivers by amounts sufficient to significantly misalign reflection events between adjacent receivers. The event misalignment is often the most serious and visible effect of near-surface irregularities, and statics correction programs are designed to correct this misalignment, in order to improve stack images.

The derivation and application of static corrections usually relies on two closely coupled concepts: surface-consistency and stationarity. Surface-consistency arises when the near-surface layer is much lower in velocity than the immediately underlying bedrock, leading to approximately vertical energy transmission into the deeper layers of the earth. In this case, all paths from a single surface source or receiver position are considered equal in length, which adds redundancy to the system of equations used to solve for statics. Normally, surface-consistency also ensures stationarity; that is, a single static shift will appropriately align all events on a single seismic trace with the corresponding events on an adjacent trace. This is because the near-surface raypaths at either source or receiver are the same, regardless of the depth of the reflection. When the velocity contrast between near-surface layer and bedrock is less, the near-surface raypaths will deviate from the vertical, and differ in length for the different reflectors; and the required static shifts will vary with reflector depth. With converted-wave data, the shear velocities in the near-surface may be so low that even nearly-vertical raypaths differ enough in length to cause apparent non-stationarity between shallow layers and deeper ones.

Another more obscure assumption underlying the application of statics to correct for near-surface variations is that each reflection event consists only of a single reflectivity function convolved with a propagating wavelet. All variations in event character due to surface-related phenomena like multi-pathing and scattering are either ignored or relegated to a separate pass of 'surface-consistent deconvolution', which attempts to equalize reflection event waveforms by removing effects common to a single surface point, like source/receiver coupling effects. In the case of multi-pathing, however, it is possible for a secondary event to be delayed from the main reflection arrival enough to turn the event into a distinct 'doublet', difficult for simple deconvolution to handle. Furthermore, with a complex reflection event like a doublet, there is no satisfactory way to align it with other non-doublet events from the same reflector using a simple time shift.

Raypath interferometry was developed to handle seismic data for which either the assumption of surface-consistency or the assumption of 'simple' reflection events breaks down (Henley, 2008, 2010, 2012). By replacing time shifting of traces with a deconvolution process, reflection events complicated by near-surface arrivals are properly handled; and the estimation of deconvolution operators using cross-correlations of raw data with 'pilot' data makes the process a kind of interferometry. The concept of surface-consistency is broadened to 'raypath consistency'; the seismic data are mapped into the radial trace (RT) domain, where deconvolution operator derivation occurs on 'common-angle' panels, making the process both raypath-consistent and nonstationary. Although raypath interferometry is a more complicated procedure than conventional residual statics estimation and application, it has been proven on data sets which both violate surface-consistency and exhibit multi-path contamination of reflections (Henley, 2012).

Because raypath interferometry uses assumptions that are generalizations of those in static correction, the method can also, without modification, be applied to data which are, in fact, surface-consistent, and which have no surface-related reflection event waveform complications. We decided to apply the method to data for which perfectly satisfactory near-surface corrections can be derived using conventional statics methods, then to compare the resulting stack images to see whether any benefits are obtained from applying the much more involved raypath interferometry instead of conventional statics. Hence, we chose two subsets of the recent Hussar low-frequency survey (Margrave et al, 2011a), since the data are of high quality and form good images. We chose to use data acquired using dynamite as a source and Vectorseis accelerometers as receivers.

PROCEDURE

Raypath interferometry

Details of the raypath interferometry procedure can be found in Henley (2008, 2010, 2012); the starting point for the procedure, like for most autostatics programs, is source (receiver) gathers which have had coherent noise attenuated, and pre-stack deconvolution applied, in this case nonstationary Gabor deconvolution (Margrave et al, 2011b). Below is a summary of the steps.

1. Apply NMO to the processed source (receiver) gathers.

2. Transform the gathers to the RT domain.

3. Sort the RT gathers to apparent velocity and surface location to form common-angle gathers.

4. Force-align the reflections on each common-angle gather, apply trace mixing to create smooth 'pilot' trace gathers.

5. For each common angle, match each pilot trace with its corresponding raw trace and cross-correlate.

6. For each common angle, derive broadband inverse filters for all cross-correlations.

7. For each common angle, convolve each inverse filter with its corresponding raw trace.

8. Sort the common-angle gathers to source position and apparent velocity, to recover the RT source (receiver) gathers.

9. Inverse transform the RT gathers to source (receiver) gathers.

10. Sort the source (receiver) gathers to receiver (source) gathers.

11. Repeat steps 2-9 above.

12. Stack the corrected gathers by CMP.

As with conventional statics, corrections are made in both the source and receiver domains, but we have found that one pass of raypath interferometry applies most of the correction, and the second pass applies any residual difference between source and receiver correction. Hence, with Vibroseis data, one pass often accomplishes nearly the whole correction; while with dynamite, a pass in the shot domain applies the shot correction and whatever portion of it that is common to the receiver at the same location, then the pass in the receiver domain applies the difference between shot and receiver correction.

We wanted to make as direct a comparison between the effects of statics correction methods on the stack image as possible, so, for the vertical component of the dynamite data (presumably PP), the identical processed source gathers that constituted the input for raypath interferometry were subjected to conventional residual statics correction and CMP stacking by Helen Isaac. For the radial dynamite component (presumably PS), however, Isaac prepared the final static-corrected CCP stack using conventional PS processing on the raw source gathers, while I used an approximate constant-CCP stacking method after raypath interferometry (complications of CCP binning aren't currently properly handled in the interferometric method). Thus, differences seen in any comparison of results for the PS data cannot necessarily be attributed strictly to the statics correction procedures, and results should be viewed as 'suggestive' but not 'conclusive'.

For both the vertical and radial components, comparison of results was primarily a subjective comparison of the features seen on the stack images.

RESULTS

Vertical component dynamite data

To emphasize the necessity for static corrections on these data, Figure 1 is the brute CMP stack of the vertical component Vectorseis dynamite data from the Hussar experiment. The source gathers have had coherent noise attenuated and Gabor deconvolution applied. A single NMO function was applied to all the shots on the line, and no statics were applied. To further enhance bandwidth and reduce random noise, Gabor deconvolution was also applied post-stack, followed by a pass of FX deconvolution. The shallow reflections on this image show ample evidence of lateral disruption, and the deeper reflections between 1.0s and 2.0s also display several disturbed zones. Conventional processing applied to the identical input gathers by Isaac, including complete NMO velocity analysis, residual statics application, and CMP stacking leads to the image in Figure 2, where two zones of possible interest at the 1100ms level are indicated (the image in the digital report can be zoomed to better see detail). Figure 3 shows the comparable CMP stack after application of raypath interferometry, while Figure 4 is the same image after application of post-stack Gabor deconvolution and FX deconvolution, whose effect is to clear the image of random, high-frequency noise, making the details more visible. Hence we use Figure 4 for comparison.
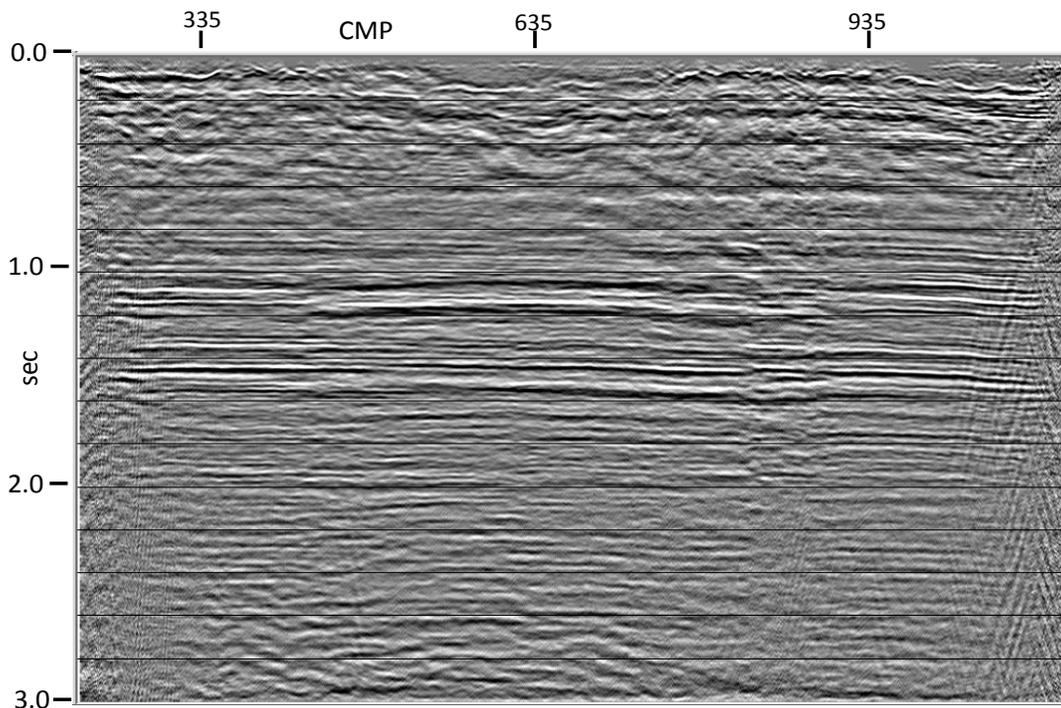

FIG.1. Brute CMP stack of Hussar vertical component dynamite Vectorseis data, with pre-stack coherent noise attenuation and Gabor deconvolution. A single stacking velocity function was applied to the entire line for NMO correction, but no statics applied. Uncorrected statics cause various image disruptions.
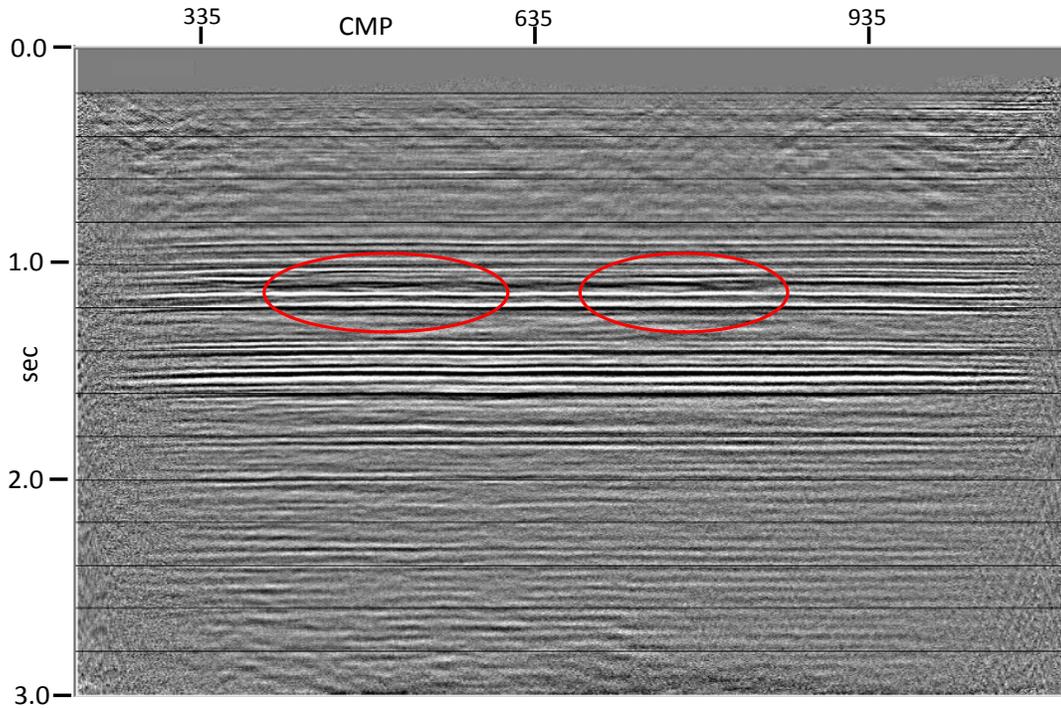
FIG.2. CMP stack image of vertical component dynamite Vectorseis data after the same pre-stack coherent noise attenuation and Gabor deconvolution as for Figure 1, but with standard NMO analysis and conventional residual statics techniques applied before stack.
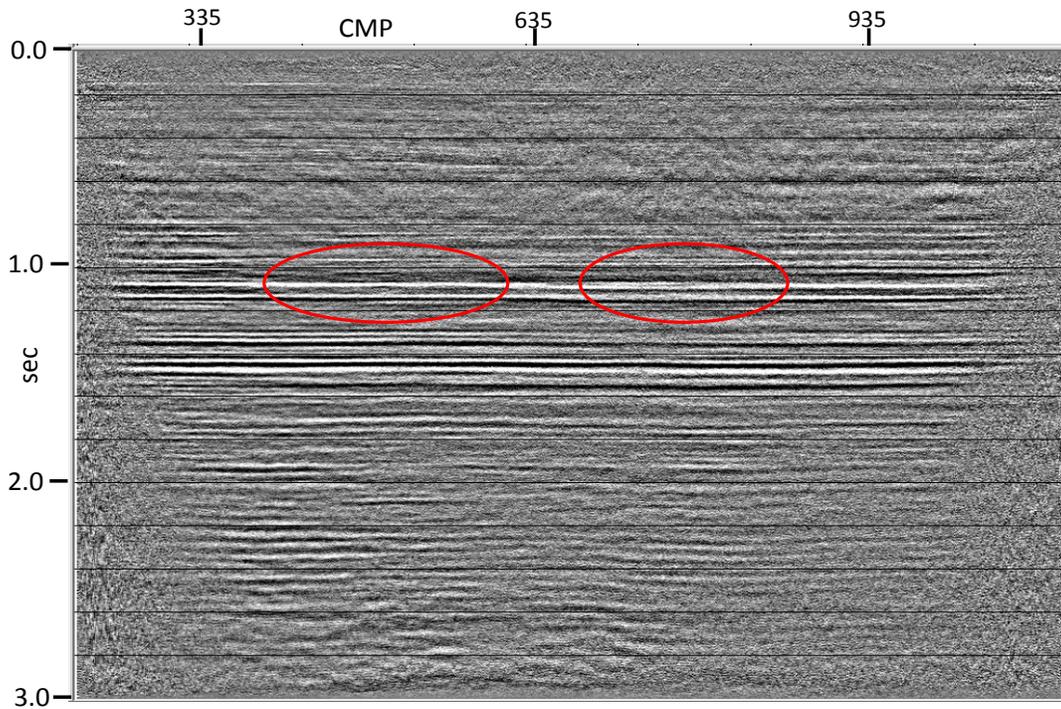

FIG.3. CMP stack image of vertical component dynamite Vectorseis data, but with raypath interferometry applied for static correction, and a single function applied for NMO correction.
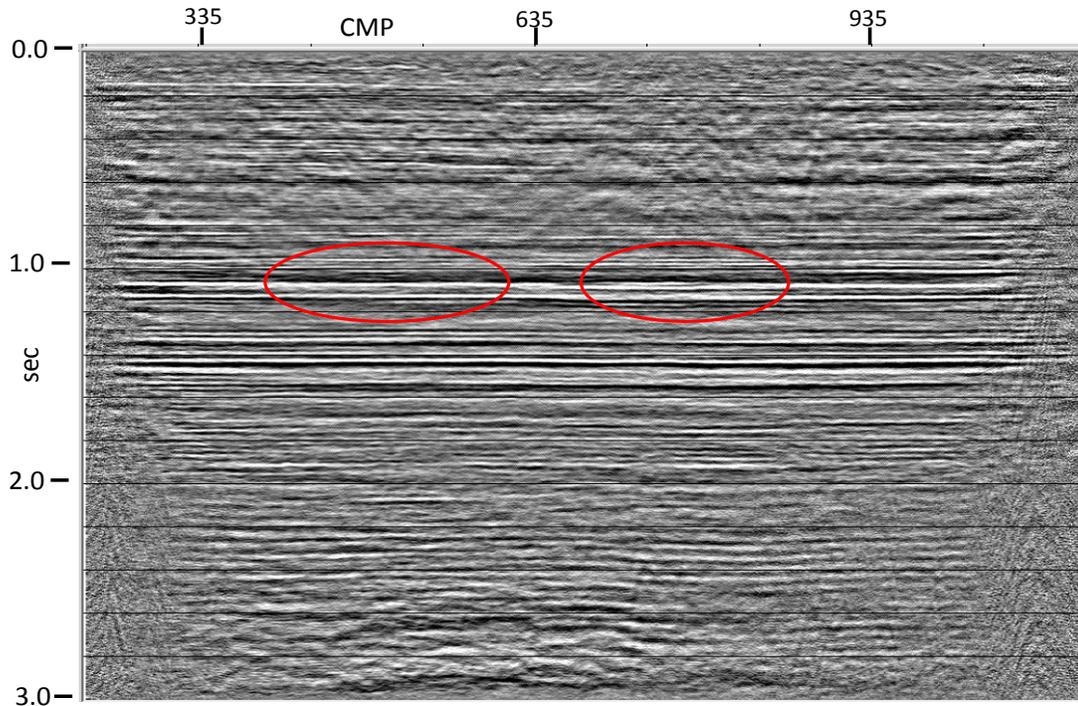
FIG.4. The same image as Figure 3, but with post-stack Gabor deconvolution and FX deconvolution applied to clean up the image.

We note first that there appears to be about 50ms of time mismatch between events on the two sections. This is likely due to no elevation or datum corrections being applied during raypath interferometry. On the conventional section, both the shallow and deep events appear fainter than those on the interferometric image in Figure 4. This is almost certainly due to the amplitude equalization due to post-stack Gabor deconvolution. The interferometric results appear to show somewhat more detail in the layering, and to have more low-frequency content. This is partly attributable to the post-stack decon, but probably due at least in part to the deconvolution nature of the interferometric statics operation. In Figure 5, we show the amplitude spectra of the section in Figure 4 as a function of surface location, while in Figure 6 we display the corresponding phase spectra. We have no comparable spectra from the image in Figure 2, however, so we can only comment in general that the vertical component dynamite image appears to contain significant energy from around 3Hz to nearly 60Hz (see also Henley, 2012b). The lateral continuity of the phase in Figure 6 at most frequencies in that range indicates that most of the 3Hz-60Hz energy is coherent reflection energy. Figure 7 is a somewhat more bandlimited version of Figure 4, and if we compare, especially, the details of the event 'braiding' within the red ellipses with that in Figure 2, it appears that the interferometric result may actually show more detail.
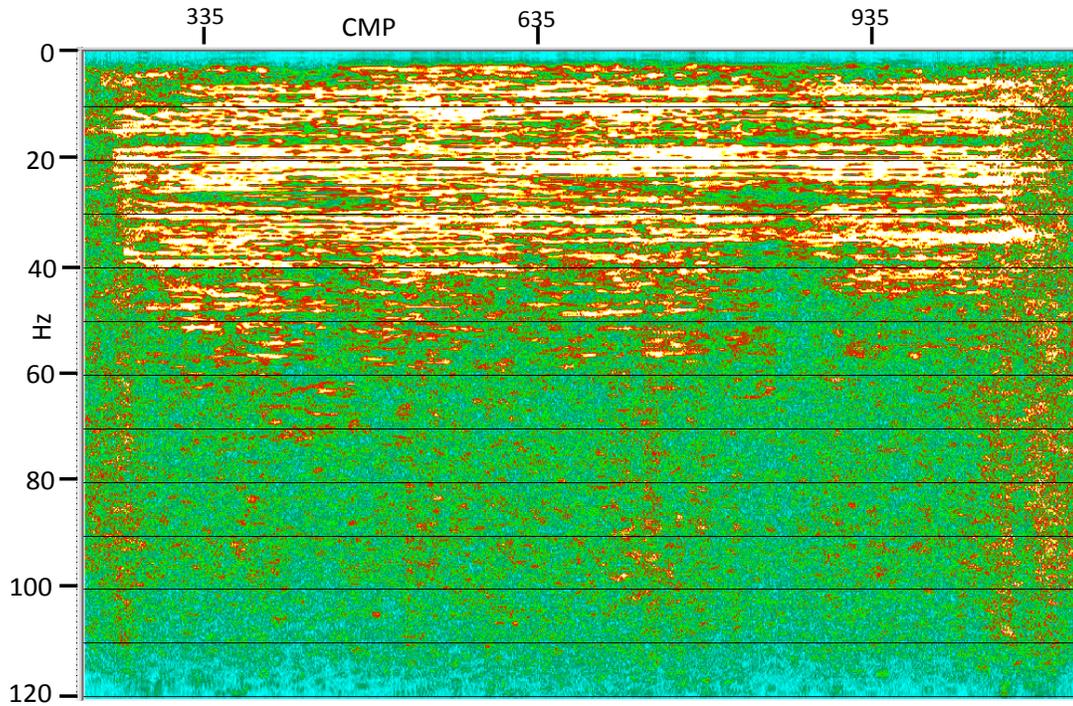
FIG.5. Amplitude spectra of the traces in Figure 4, plotted against CMP. High spectral amplitudes extend from about 3Hz to nearly 60Hz.
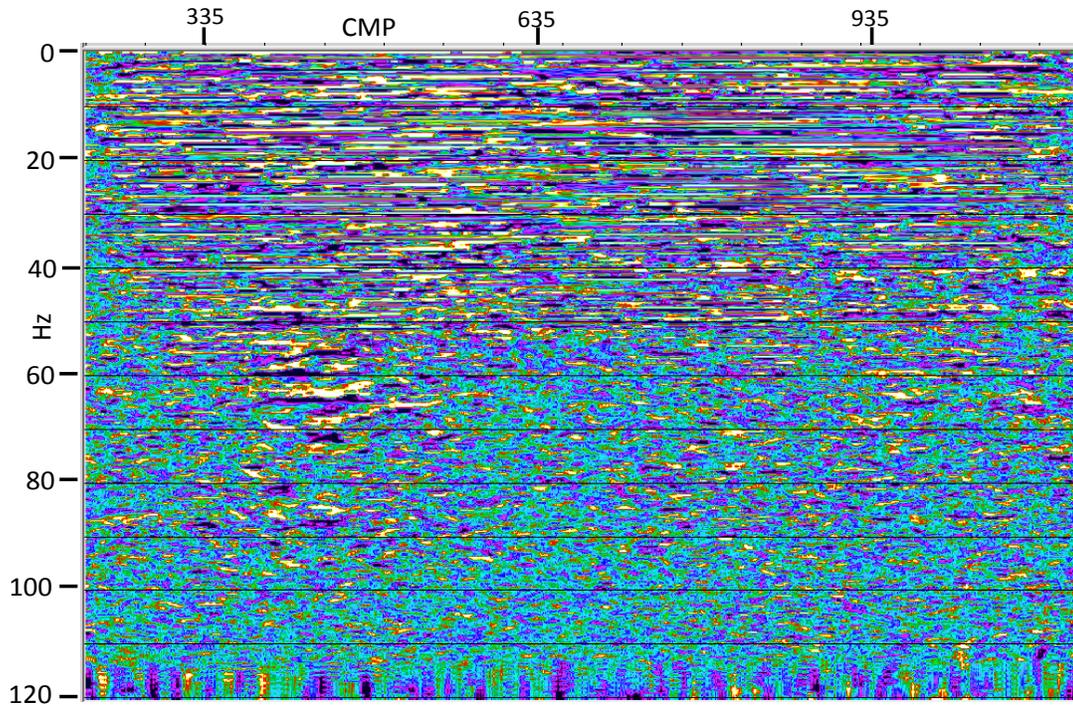

FIG.6. Phase spectra of the traces in Figure 4 plotted against CMP. Lateral continuity of frequency components implies that frequencies between 3Hz and 60Hz are part of the coherent seismic reflection signal.
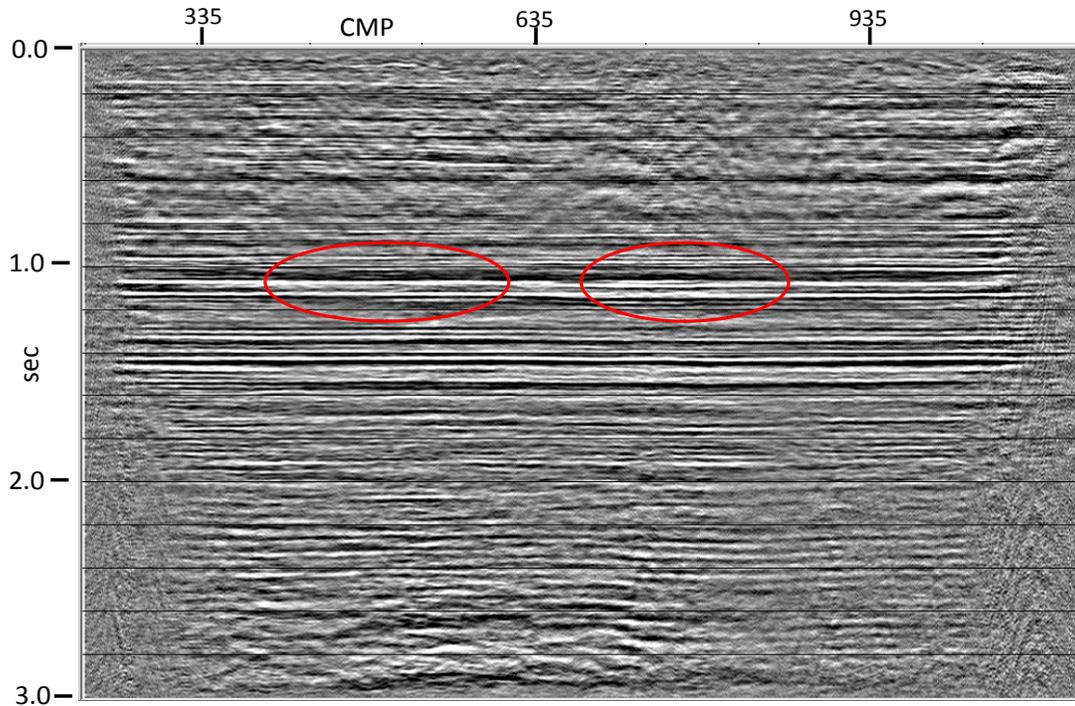
FIG.7. Slightly bandlimited version of the image in Figure 4. Details of the 'braiding' of the reflection event at about 1.0s should be compared with the same features on Figure 2.

Radial component dynamite data

As in the comparison for the vertical component, we show a brute CCP stack of the radial component of the Hussar Vectorseis dynamite data in Figure 8. As with the vertical component, the source gathers were pre-processed for coherent noise and deconvolved with Gabor deconvolution. Rather than attempt rigorous CCP binning on these data, we assigned an approximate CCP for each trace (2/3 of the offset between source and receiver). Also, we elected to use regular NMO correction with a single NMO velocity function, rather than attempt to be more theoretically correct. Hence, our results may differ from those produced by Isaac for the same data at least partly because we're stacking differently. Nevertheless, in Figure 8, we can see evidence of image disruption due to improper near-surface corrections, particularly in the shallow section. It should be noted here that events shallower than about 400ms may not be PS events, but could well be leakage of PP reflections into the radial component at the more oblique angles. Just to confirm what we suspect about the presence of receiver-side shear statics, Figure 9 shows a common-receiver stack of the radial component, where large statics anomalies are visible at several locations along the line. Figure 10 is the conventionally processed CCP stack of these input data, provided by Isaac after a successful application of PS statics. In comparison, Figure 11 displays our approximate CCP stack after raypath interferometry. As in the vertical component comparison, post-stack Gabor deconvolution and FX deconvolution have been applied.
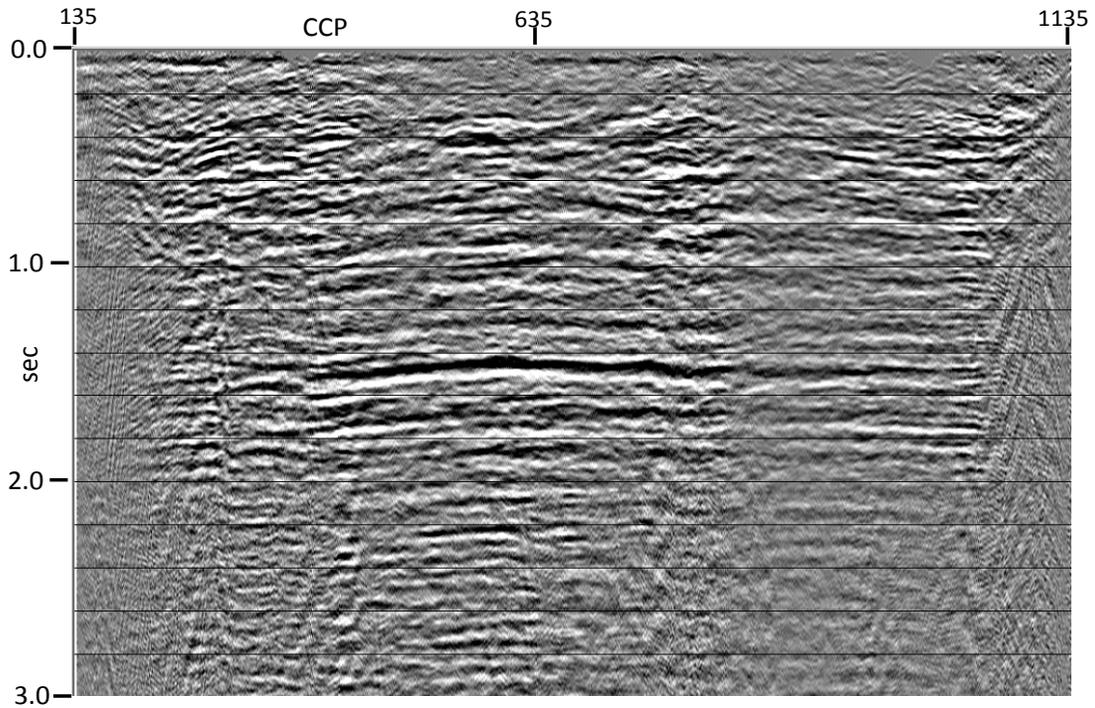
FIG.8. Approximate CCP stack of radial component dynamite Vectorseis data from Hussar, using a single velocity function for NMO correction. No statics have been applied.
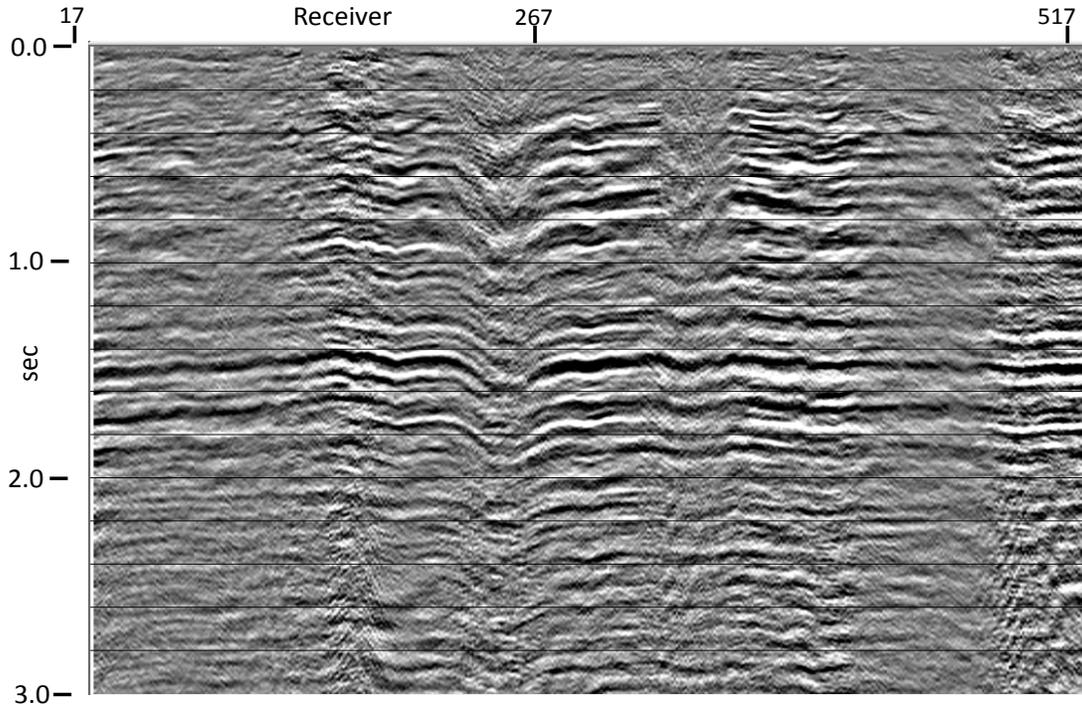

FIG.9. Common-receiver stack of radial component dynamite Vectorseis data from Hussar. On this image, large receiver statics (S-wave statics) can be readily seen.
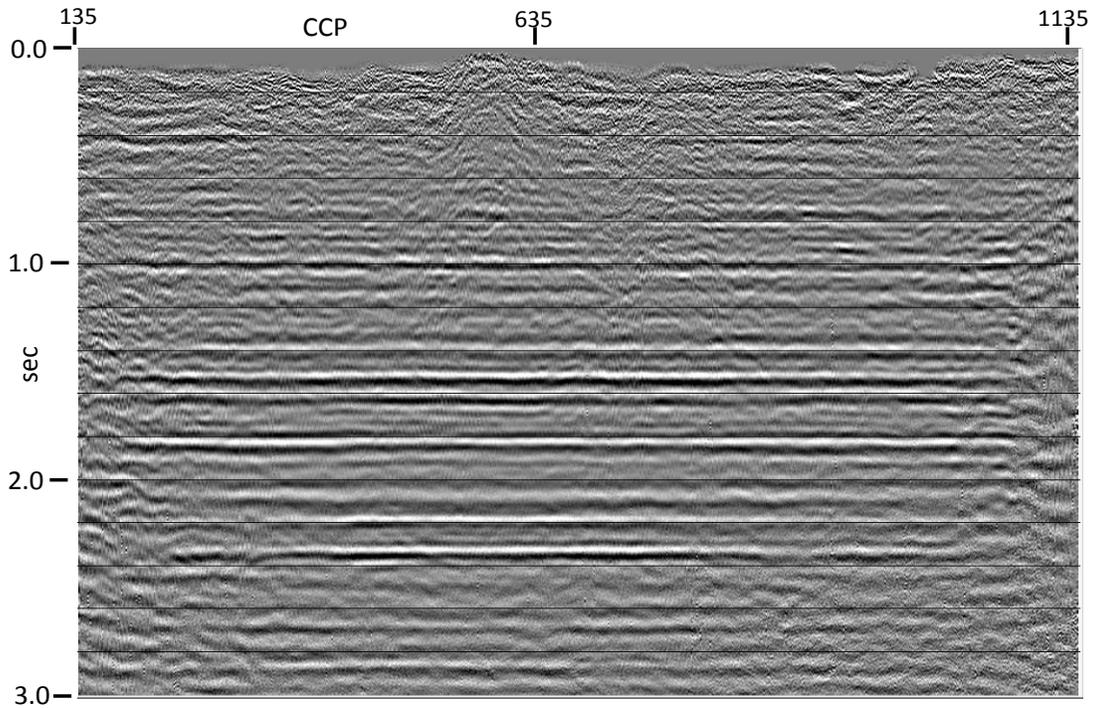
FIG.10. CCP stack of radial component dynamite Vectorseis data. Conventional processing has been applied, including CCP binning, NMO analysis and correction, and conventional converted-wave static correction procedures.
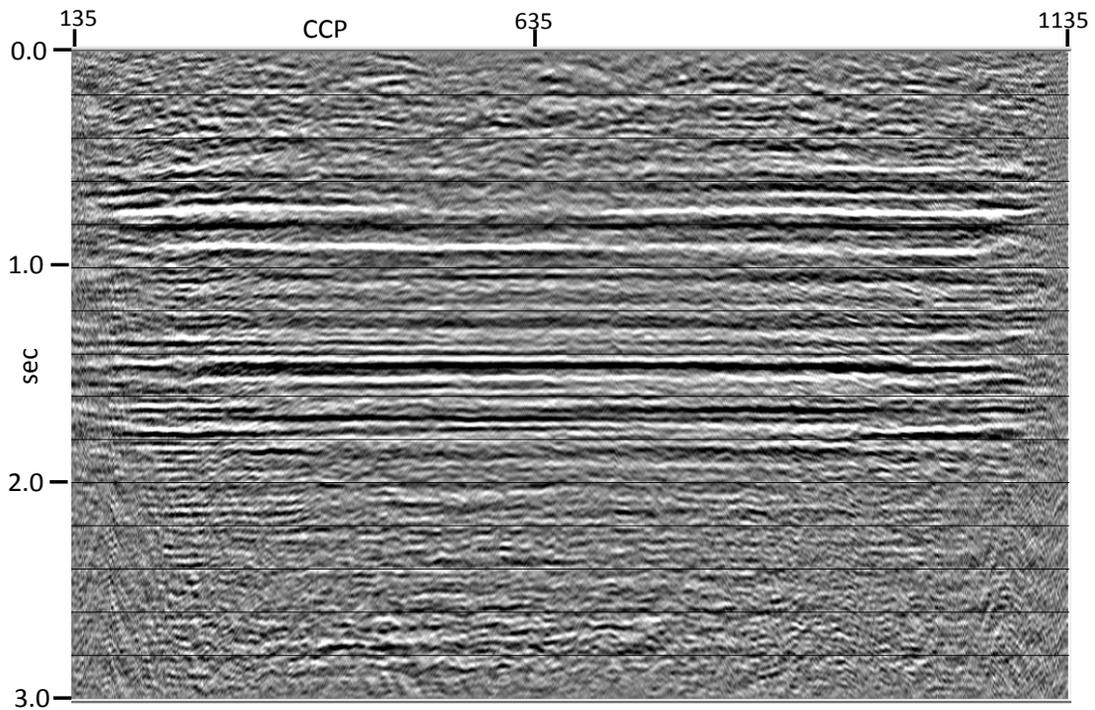

FIG.11. Approximate CCP stack of radial component dynamite Vectorseis data after raypath interferometry for applying static correction. Single velocity function used for NMO correction.
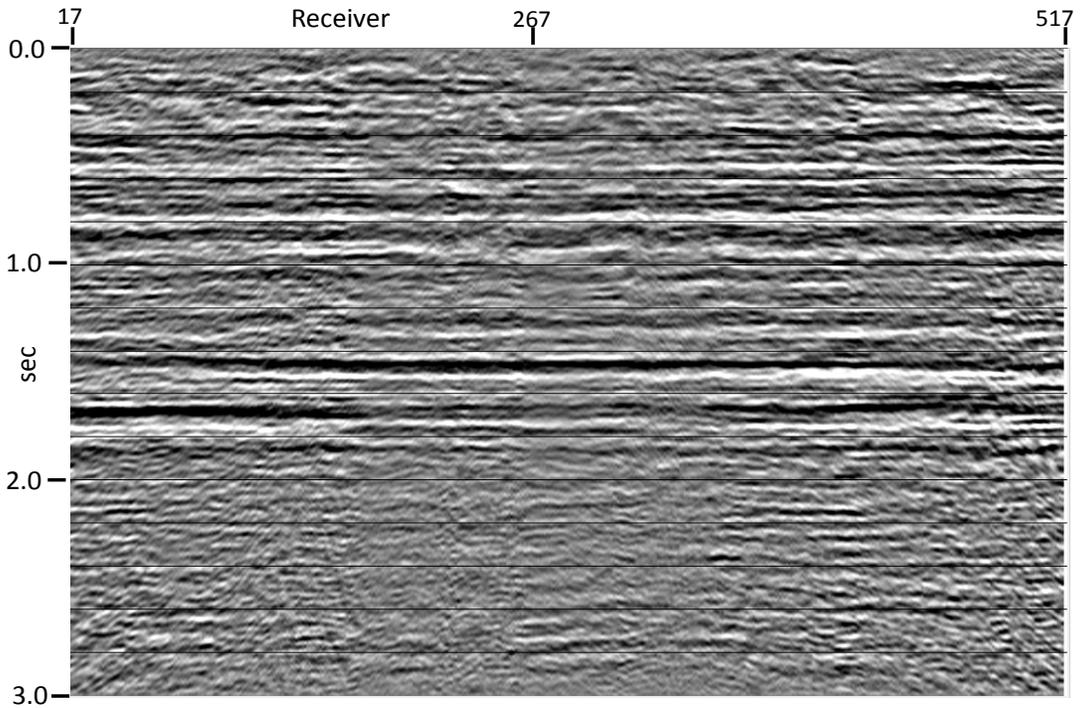
FIG.12. Common-receiver stack of radial dynamite Vectorseis data after raypath interferometry.
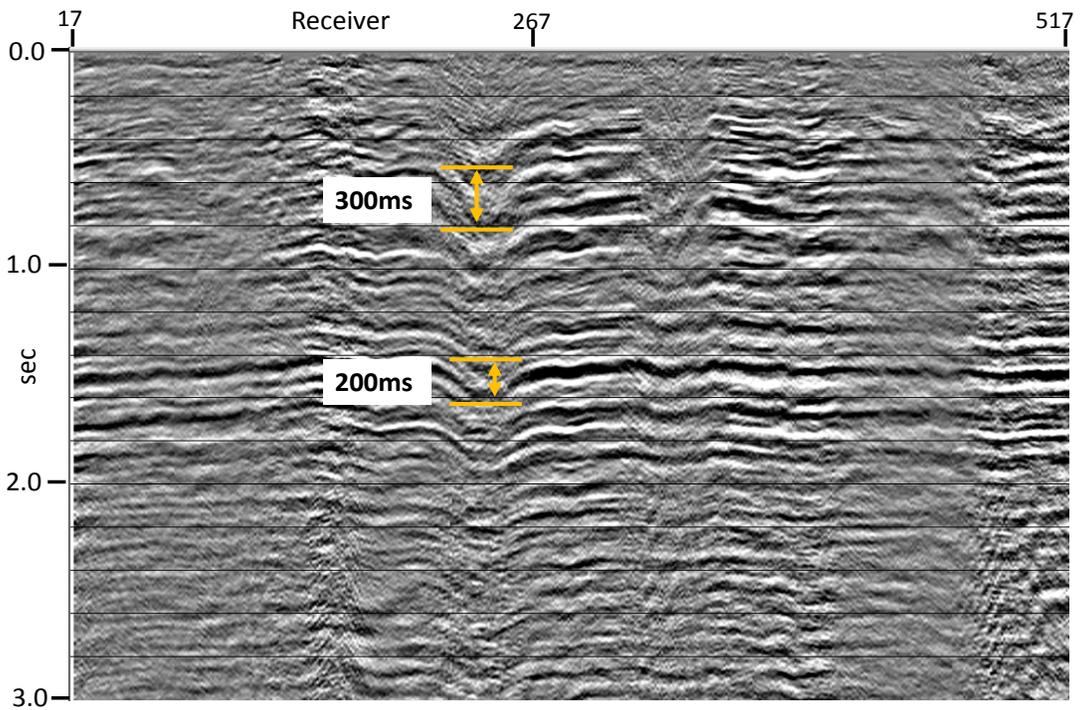

FIG.13. Common-receiver stack in Figure 9 showing relative size of statics anomalies at different depths in the section.

There are certainly more differences between these two images than between the ones in our vertical component comparison, but we hesitate to make any very strong comments about the significance of these differences, given the very real differences in creating the CCP stacks. In general, for the portion of the image between 800ms and 2000ms, the interferometric results seem to show more layer detail and have a more broadband appearance. On the other hand, prominent events below 2000ms on the conventional CCP stack are almost entirely missing on the interferometric result; and we see events at around 800ms and above on the interferometric result that are much weaker on the conventional result. We have no explanation for this at present, except to conjecture that the correlation window length and weighting parameters in raypath interferometry are likely involved.

Confirmation of the success of raypath interferometry can be seen on the common-receiver stack shown in Figure 12, which now shows no static anomalies, after raypath interferometry. As a point of interest, Figure 13 shows the common-receiver stack before raypath interferometry, with overlaid indicators of the magnitude of the static anomalies at two different levels. In comparison with Figure 12, we see that these different-sized anomalies were corrected concurrently by interferometry, which helps explain the strength of the events at this level on the Image in Figure 11, and possibly the weakness of the same events on Figure 10. Note, as well, some evidence of discontinuity for these events on Figure 10.

DISCUSSION

It is too early to draw any definitive conclusions from comparisons of conventional statics and raypath interferometry, because we've not optimized the results of both approaches and made them as directly comparable as possible, particularly for the radial component results. Nevertheless, we see intriguing hints that the interferometric approach may, in some cases, help preserve or even enhance signal bandwidth.

ACKNOWLEDGEMENTS

REFERENCES

Henley, D.C., 2008, Raypath interferometry: statics in difficult places, 78th Annual international meeting, SEG, Expanded abstracts, 1263-1267.

Henley, D.C., 2010, Hybrid raypath interferometry: correcting converted wave receiver statics, 80th Annual international meeting, SEG, Expanded abstracts, 1861-1865.

Henley, D.C., 2012, Interferometric application of static corrections, Geophysics, **77,** No. 1, Q1-Q13.

Henley, D.C., 2012, Where in the earth are the low frequencies: comparison of sources at Hussar, 2012 CREWES research report, **24.**

Margrave, G.F., Mewhort, L., Phillips, T., Hall, M., Bertram, M.B., Lawton, D.C., Innanen, K.A.H., Hall, K.W., and Bertram, K., 2011, The Hussar low-frequency experiment, 2011 CREWES research report, **23**.

Margrave, G.F., Lamoureux, M.P., and Henley, D.C., 2011, Gabor deconvolution: Estimating reflectivity by nonstationary deconvolution of seismic data, Geophysics, **76,** No. 3, pp W15-W30.